

arXiv:2512.02301v1 [cs.CR] 2 Dec 2025

arXiv:2512.02301v1 [cs.CR] 2 Dec 2025

arXiv:2512.02301v1 [cs.CR] 2 Dec 2025

arXiv:2512.02301v1 [cs.CR] 2 Dec 2025

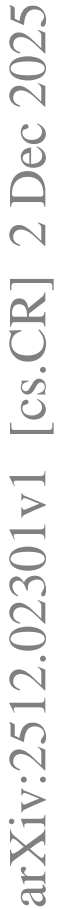
arXiv:2512.02301v1 [cs.CR] 2 Dec 2025

arXiv:2512.02301v1 [cs.CR] 2 Dec 2025

arXiv:2512.02301v1 [cs.CR] 2 Dec 2025

arXiv:2512.02301v1 [cs.CR] 2 Dec 2025

arXiv:2512.02301v1 [cs.CR] 2 Dec 2025



arXiv:2512.02301v1 [cs.CR] 2 Dec 2025

arXiv:2512.02301v1 [cs.CR] 2 Dec 2025

arXiv:2512.02301v1 [cs.CR] 2 Dec 2025

arXiv:2512.02301v1 [cs.CR] 2 Dec 2025

arXiv:2512.02301v1 [cs.CR] 2 Dec 2025

frameworks.

Recent research has explored various aspects of this domain. Li et al. [13] developed quantum protocols to prevent gradient inversion attacks through private inner-product estimation and quantum state concealment. In classical federated learning, Behera et al. [14] proposed large model-assisted approaches for edge-based object detection, while Kishawy et al. [15] focused on lane segmentation systems. However, these works do not address the comprehensive integration of quantum computing, differential privacy, and quantum-secure communications necessary for next-generation autonomous vehicle networks.

In this paper, we present vQFL as a *proof of concept*, as shown in Figure 1, implementing the Quantum Vanguard concept through a novel framework that combines quantum computational advantages with multi-layered privacy and security guarantees. Our approach specifically addresses the computational, privacy, and security challenges of autonomous vehicle fleets while establishing a foundation for quantum-resistant intelligent transportation systems.

A. Contribution

The contributions of this work are listed below.

- 1) We propose a novel vehicular quantum federated learning (vQFL) framework for autonomous vehicle driving networks for distributed quantum machine learning. Our proposed framework (vQFL) provides privacy on top of default data privacy provided by QFL framework and secure communication means through QKD.
- 2) We further propose and investigate the concept of fine-tuning, or optimizing, the global model after the averaging phase through additional customizations. This procedure aims to achieve improved performance at both the local and global model levels and is evaluated via experimental analysis, referred to as server-side optimized vehicular QFL (ft-vQFL).
- 3) We present extensive theoretical and experimental analysis to demonstrate the practicality and adaptability of the proposed method in the field of autonomous vehicle technology with the Qiskit framework utilizing various models such as VQC, QCNN, and samplerQNN in various datasets including KITTI, nuScenes, and Waymo datasets.

B. Originality and novelty

Figure 1 presents an architectural overview of our proposed vQFL framework, illustrating the sophisticated integration of quantum computing paradigms with autonomous vehicle technology. The architecture depicts a network of connected autonomous vehicles (Tesla, Waymo, and other manufacturers) equipped with onboard quantum processors that collect and process multi-modal sensor data streams (high-definition LIDAR point clouds, multi-camera arrays, millimeter-wave radar, GPS, and inertial measurement units) locally.

Each vehicle in Figure 1 independently trains quantum machine learning models, including variable Quantum Circuits (VQC), Quantum Convolutional Neural Networks (QCNN),

and our samplerQNN (Quantum Neural Network) on its private driving data. This localized training approach ensures that sensitive driving behaviors, route patterns, and environmental observations never leave the vehicle's secure computing environment.

The framework of Figure 1 implements our novel three-tiered security approach: (1) Base-level QFL Privacy: Inherent data privacy from the federated architecture where only model parameters not raw data are shared; (2) Differential Privacy Layer: Application of calibrated Laplacian or Gaussian noise (ϵ) to model parameters before transmission, mathematically guaranteeing protection against model inversion and membership inference attacks; (3) Quantum Cryptographic Layer: Implementation of BB84 quantum key distribution protocol that leverages quantum superposition and measurement principles to establish information-theoretically secure communication channels. These encrypted model can be transmitted either to a central server in a hierarchical client-server topology or directly between vehicles in a decentralized peer-to-peer network, depending on deployment requirements and available infrastructure.

The system illustrated in Figure 1 performs intelligent federated aggregation of these quantum-secure updates to create an improved global model. This model benefits from collective learning across diverse driving scenarios (urban environments, highways, adverse weather conditions) while maintaining strict privacy guarantees and quantum-resistant security. The bidirectional arrows in Figure 1 represent the secure exchange of model parameters, with quantum-encrypted channels ensuring protection against both conventional cryptanalytic attacks and future quantum computing threats. The vQFL framework supports both synchronous and asynchronous communication patterns to accommodate varying connectivity conditions in real-world vehicular networks.

II. PRELIMINARIES AND BACKGROUND

The convergence of quantum computing and autonomous vehicle technology creates new opportunities to address critical challenges in vehicular networks. Autonomous vehicles generate massive data volumes (20-40 TB daily per vehicle) that must be processed with ultra-low latency for safe operation [12]. These vehicles rely on sophisticated perception systems for object detection, lane segmentation, and trajectory prediction under various environmental conditions [16], [17].

QFL offers a promising approach by extending classical federated learning with quantum computational capabilities [18]. QFL employs parameterized quantum circuits, quantum data encoding, and qubit-based processing within a hybrid quantum-classical framework where quantum circuits perform computations while classical optimizers update the circuit parameters [4]. This paradigm leverages quantum mechanical phenomena superposition, entanglement, and interference to potentially accelerate specific computational tasks relevant to autonomous driving.

However, collaborative learning in vehicular networks introduces significant privacy and security concerns. Differential privacy (DP) addresses these challenges by providing mathematically rigorous privacy guarantees, ensuring that model

TABLE I: Selected related work in FL for AVs

Work	Technique	Features	Model	Simulation	Datasets	Type
Semi-SynFed [22]	Semi-synchronous FL	Select appropriate nodes, dynamic waiting time, dynamic aggregation scheme	Classical	Open datastreet	FMNIST, CIFAR10, TSRD	CNN
LMFL [14]	Large Model assisted FL	Object detection, synchronous/asynchronous approach, hierarchical structure	Classical	TensorFlow	KITTI	LENET
FedLane [15]	Secure and Efficient FL	Lane Segmentation, real-time inference, complicated road scenarios	Classical	TensorFlow	TuSimple, CULane	U-Net, ResUNet etc.
Copilot4D [17]	World Models for AV via Discrete Diffusion	Unsupervised world models, Use discrete Diffusion, tokenize sensor observations, prediction via discrete diffusion	Classical	-	nuScenes, KITTI, Argoverse 2	Discrete Fusion Model, VQVAE-like
BDFL [23]	BFT decentralized FL	Privacy Preserving, Peer-to-peer, HydRand protocol, PVSS Scheme, Multi-Object recognition, Privacy Preserving	Classical	PyTorch	MNIST, KITTI	MultiLayer Perceptron Model, CNN
FADNet [24]	Deep FL for AD	Peer to peer deep FL, decentralized, Model Stability, Convergence, Handle Imbalance data	Classical	Carla, Gazebo	Udacity data	silo Model
This work	Vehicular QFL	Quantum private and secure QFL	Quantum	Qiskit	nuScenes, Waymo, KITTI	VQC

outputs differ by at most a factor of e^ϵ (with exception probability δ) when trained on datasets differing by a single record [19], [20]. For communication security, QKD enables information-theoretically secure key exchange based on quantum mechanical principles, making it resistant to both classical and quantum attacks [21].

The integration of these technologies, QFL, differential privacy, and QKD creates a comprehensive framework to address the unique challenges of autonomous vehicles: computational efficiency for real-time decision making, preservation of privacy for sensitive driving data, and quantum-resistant security for vehicle-to-vehicle and vehicle-to-infrastructure communications [3], [15]. We aim to explore and exploit such a joint framework to establish a foundation for next-generation autonomous vehicle systems that can operate securely and efficiently in the post-quantum era.

A. Literature

The technological progress of autonomous vehicles has surpassed human expectations, with notable implementations and services already being offered by major tech companies such as Waymo Taxi and Tesla Robotaxi. One of the main reasons for this is the considerable developments and advances in the field of artificial intelligence, particularly deep learning [25]. In this section, we conclude various works done in the field of machine learning for autonomous vehicles specifically focusing primarily on federated distributed learning.

Some recent work, also shown in Table I, in the field of classical FL includes the semi-synchronous FL protocol with dynamic aggregation on the Internet of Vehicles [22]. The key idea behind the proposed solution is to improve machine learning performance and efficiency through steps like first selecting appropriate nodes for dynamic asynchronous aggregation based on computational capacity, network capacity, etc. Similarly, in terms of object detection, Behera et al. [14] proposed a large model-assisted FL for object detection for the autonomous vehicle in edge. The work focuses on combining the strength of both synchronous and asynchronous methods and further organizing devices into a hierarchical structure to optimize model convergence, as well as to mitigate any

stragglers and dropout problems. In terms of lane segmentation, Kishawy et al. [15] proposed the secure and efficient FL system, FedLane, for AV for complicated and dynamic road scenarios. Zhang et al. [17] proposed unsupervised world models, Copilot4D, for AV using discrete diffusion. It is a world-modeling approach in which sensor observations are first tokenized with VQVAE and prediction is then performed through discrete diffusion. Other works include BDFL, a Byzantine fault-tolerant decentralized FL for AVs by Chen et al. [23]. It is a decentralized FL approach for privacy-preserving addressing multi object recognition task etc.

Nguyen et al. [24] proposed the peer-to-peer deep FL approach to train deep architectures in a decentralized manner and design a new federate AV network (FADNet) to improve model stability, convergence, etc. Xu et al. [26] proposed secure FL for quantum autonomous vehicle networks based on the QKD protocol, the SAGIN-enabled QAVN model, and the FL framework.

From the start of machine learning approaches such as the transportable neural network approach to AVs [27], the integrated framework for decision making and motion planning for AVs [28] to different decentralized approaches in AVs including FL, the key consideration and network are in a classical form similar to conventional computing. Considering recent advances in the field of quantum computing and additional threat to quantum attacks on classical computers and classical problems, it would be an overstatement that a novel quantum proof and a quantum way of decentralized approaches is integral to the survival and adaptation of the AV industry in the quantum era. Thus, our work fundamentally is different from all the related works and as far as we know is the first work towards quantum FL for AVs with SOTA real-world datasets such as Waymo, KITTI, nuScenes etc.

III. PROPOSED VEHICULAR QFL

We introduce a secure and privacy-preserving framework for vehicular quantum federated learning (vQFL). This framework is comprised of three primary components:

- 1) A QFL framework tailored for self-driving vehicles.
- 2) A privacy-preserving strategy applied to QFL models.
- 3) A secure QKD communication protocol for QFL.

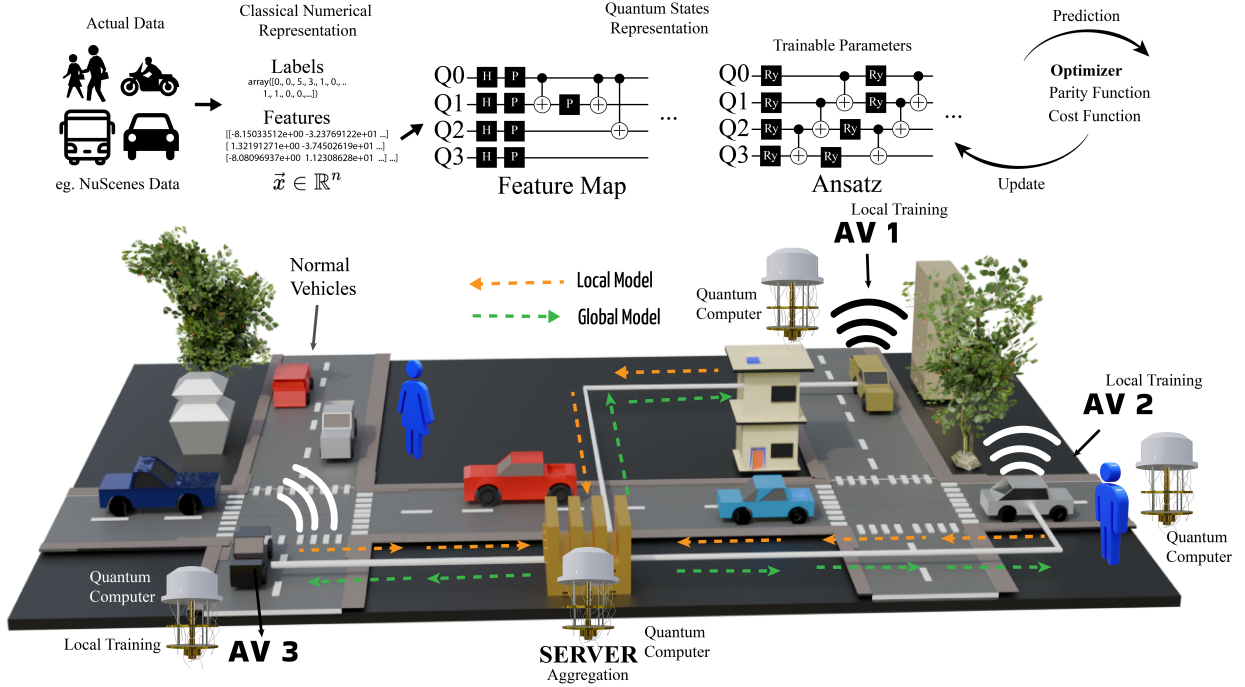


Fig. 2: *Proposed privacy-preserving secure vehicular QFL Framework: Autonomous vehicles collaboratively train global model; vQFL framework integrates quantum computing with autonomous vehicle technology. The architecture involves connected vehicles with onboard quantum processors training models locally on private driving data. Our three-tiered privacy and security approach combines: (1) Base-level QFL privacy where only model parameters are shared; (2) Differential privacy layer applying calibrated noise to parameters; and (3) Quantum cryptographic layer implementing BB84 protocol for secure communications. The system can be extended to both client-server and peer-to-peer topologies, enabling collaborative intelligence while maintaining quantum-resistant security.*

We propose a QFL framework for a vehicular scenario where autonomous vehicles can locally train on their data facilitating distributed machine learning with access to quantum computational capability. The Algorithm 1 shows the main steps involved in the vehicular QFL framework in terms of coordination between vehicles and the server, along with some other details such as topology, data distribution, etc.

In our proposed framework, we implement privacy measures for model where we add noise to the model parameters. This step helps prevent any adversary or malicious server from inferring information from the model about the data that were trained, which is presented in Algorithm 2. On top of default QFL and privacy protocol, we add additional layer providing security with QKD implementation mechanism that works with QFL framework. Our design involves creating QKD secret keys, encryption, and decryption, etc. which are detailed in Algorithm 3.

With QKD, we encrypt the model weights before sending them to the server and vice versa. The model weights are differentially private before encryption and thus maintaining multi layer privacy and security to the communication framework. In this work, we have followed the BB84 protocol for QKD [29]. Clients and server are connected through the quantum channel, where they exchange qubits which are processed to generate encryption and decryption key (symmetric key) to send private message using the classical channel by using methods like one-time padding.

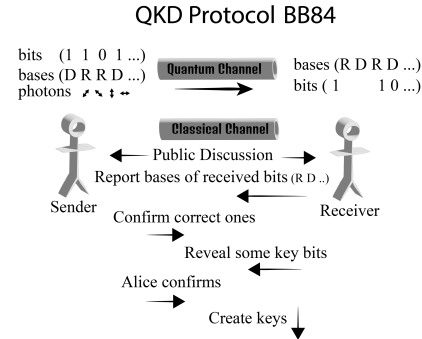


Fig. 3: QKD Protocol: Standard BB84 protocol for Quantum Key Distribution [29].

The implemented protocols are as follows: For message m , random binary strings $\in \{0, 1\}^N$ of length s are generated simulating a quantum circuit where the H gate is applied to each of the s qubits initialized to $|0\rangle$, and then measured in the Z base to obtain random bits. Mathematically, for length s , initialize qubits $|\psi_0\rangle = |0\rangle^{\otimes s}$ and then apply the Hadarmard gate as

$$|\psi\rangle = H^{\otimes s}|\psi_0\rangle = \bigotimes_{j=1}^s \frac{1}{\sqrt{2}}(|0\rangle + |1\rangle)_j.$$

The measurement in Z-basis results in outcome sequence $R = (r_j)_j^s$, where $r_j = 0$ or 1 with the probability of $\frac{1}{2}$

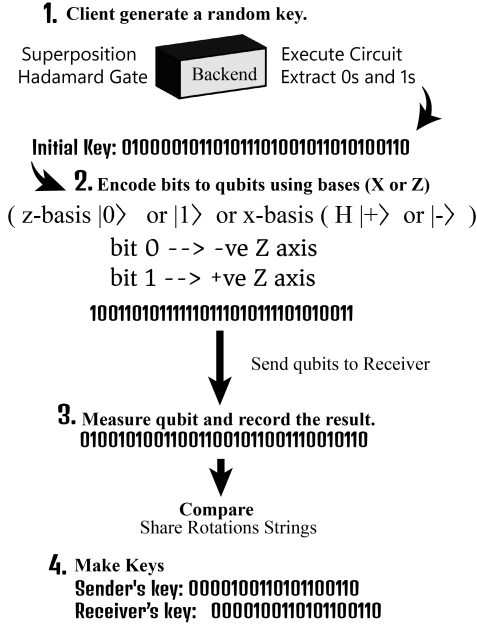


Fig. 4: QKD Generation: Key Generation implemented in this work using backend and following BB84 Protocol.

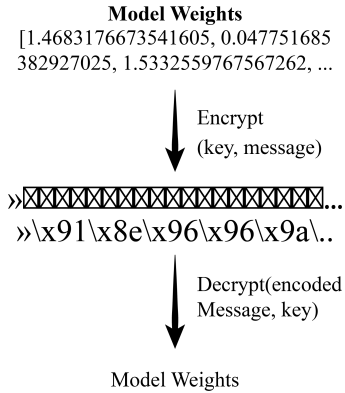


Fig. 5: QKD Encryption: Encryption and Decryption of model weights as performed in the work (sample preview)

independent (uniform over $\{0, 1\}^s$). Now, a random initial key is generated D^A along with the sender's basis choices (B^A) and the receiver's basis choices (B^B).

Each client device prepares N qubits based on their bits $D^A = (d_j^A)_{j=1}^N$ and bases $B^A = (b_j^A)_{j=1}^N$. However, server measures using bases $B^B = (b_j^B)_{j=1}^N$. Mathematically, For each position $j = 1$ to N , the Device prepares the j^{th} qubit as,

$$|\psi\rangle = H^{b_j^A} X^{d_j^A} |0\rangle \quad (1)$$

such that

- If $b_j^A = 0$ (rectilinear basis): $|\psi_j\rangle = |d_j^A\rangle$ ($|0\rangle$ or $|1\rangle$).
- If $b_j^A = 1$ (diagonal basis): $|\psi_j\rangle = H|d_j^A\rangle = \begin{cases} |+\rangle & \text{if } d_j^A = 0, \\ |-\rangle & \text{if } d_j^A = 1. \end{cases}$

The qubit is transmitted to the server. After receiving it, the

Algorithm 1 Privacy-Preserving Quantum-Secure vQFL

- Notations:**
- K : Number of clients, indexed $k = 1, \dots, K$; S : Central server.
- $\mathcal{D}_k = \{(x_i^{(k)}, y_i^{(k)})\}_{i=1}^{n_k}$: Local dataset of client C_k , size n_k .
- Model types: $m \in \{\text{VQC}, \text{QCNN}, \text{SamplerQNN}\}$.
- Global parameters at round t : $\theta^{(t)}$; Local loss: $\mathcal{L}_k(\theta) = \frac{1}{n_k} \sum_{i=1}^{n_k} \ell(\theta; x_i^{(k)}, y_i^{(k)})$.
- Optimizers: Gradient-based (e.g., Quantum Natural Gradient) or gradient-free (e.g., COBYLA).
- DP parameters: (ϵ, δ) , noise $\mathbf{z}_k \sim \mathcal{N}(0, \sigma^2 \mathbf{I})$.
- QKD for secure key generation; T : Number of rounds.
- Initialize:** Server sets $\theta^{(0)}$, broadcasts to clients via QKD channels.
- for** $t = 1$ to T **do**
- for each client** C_k **in parallel do**
- Receive $\theta^{(t-1)}$.
- Local training: Update $\theta_k^{(t)}$ to minimize $\mathcal{L}_k(\theta)$.
- Gradient-based: $\theta_k^{(t)} \leftarrow \theta^{(t-1)} - \eta \nabla_{\theta} \mathcal{L}_k(\theta^{(t-1)})$.
- Gradient-free: $\theta_k^{(t)} = \arg \min_{\theta} \mathcal{L}_k(\theta)$.
- Add DP noise: $\tilde{\theta}_k^{(t)} \leftarrow \theta_k^{(t)} + \mathbf{z}_k, \sigma \propto \frac{\sqrt{\ln(1.25/\delta) \cdot C}}{\epsilon n_k}$.
- Send $\tilde{\theta}_k^{(t)}$ to server via QKD channel.
- Server:** Compute $\theta^{(t)} \leftarrow \frac{1}{\sum_k n_k} \sum_{k=1}^K n_k \tilde{\theta}_k^{(t)}$.
- Optimize global model (if desired).
- Broadcast $\theta^{(t)}$ via QKD channels.
- Focus:** DP noise ensures privacy against model inversion; QKD provides quantum-secure parameter exchange.

Algorithm 2 Privacy Mechanism

- Input:** Model parameters $\theta = [\theta_1, \theta_2, \dots, \theta_n]$, privacy budget $\epsilon > 0$, sensitivity $\Delta \geq 0$
- Output:** Noisy parameters $\tilde{\theta} \in \mathbb{R}^n$
- procedure** ADDDPNOISE(θ, ϵ, Δ)
- Train local model to obtain parameters $\theta \in \mathbb{R}^n$.
- Determine parameter shape $n = |\theta|$.
- Compute noise scale $\sigma = \frac{\Delta}{\epsilon}$.
- Generate noise $\eta \sim \text{Laplace}(0, \sigma)^n$.
- Compute noisy parameters $\tilde{\theta} = \theta + \eta$.
- return** $\tilde{\theta}$

server applies its basis transformation

$$|\phi_j\rangle = H^{b_j^B} |\psi_j\rangle$$

and measures $|\phi_j\rangle$ in z-basis and get outcome $r_j \in \{0, 1\}$, with probability $|\langle r_j | \phi_j \rangle|^2$. The server result is equal to $R^B = (r_j)_{j=1}^N$. The bases B^A and B^B are shared publicly whereby bits that matches bases match are kept.

Let $S = \{j \in \{1, \dots, N\} \mid b_j^B = b_j^A\}$ (expected $|S| \approx N/2$). Then, keys are generated on the basis of the bases and results of measurements.

For our model weights θ_i in the form $[m_1, m_2, m_3 \dots m_n]$ for the client i , the secret key generated using the QKD protocol $K = k_1 k_2 \dots k_s$ for length s where $n = s$ after shortening the

Algorithm 3 Security Protocol

```

1: Input: Message  $m \in \{0, 1\}^n$ , desired key length  $n$ 
2: Output: Ciphertext  $c \in \{0, 1\}^n$ , decrypted  $m' \in \{0, 1\}^n$ 
3: procedure RANDOMSTRINGGEN( $n$ )
4:   Initialize quantum backend  $\mathcal{B}$ .
5:   Define registers  $Q = \{q_i\}_{i=1}^n$ ,  $C = \{c_i\}_{i=1}^n$ .
6:   Construct quantum circuit  $\mathcal{C}$ , applying  $H^{\otimes n}$  to  $Q$ .
7:   Execute  $\mathcal{C}$  on  $\mathcal{B}$ , get bit string  $s \in \{0, 1\}^n$ .
8:   Generate bases  $b_A, b_B \in \{X, Z\}^n$  for both.
9:   Encode qubits with  $s, b_A$ : apply  $X$  if  $s_i = 1$ ,  $b_{A,i} = X$ .
10:  Transmit encoded qubits  $|\psi\rangle = \bigotimes_{i=1}^n |\psi_i\rangle$  to receiver.
11:  Measure qubits in basis  $b_B$  to get  $s' \in \{0, 1\}^n$ .
12:  Shift: keep bits where  $b_{A,i} = b_{B,i}$ , get key  $k \in \{0, 1\}^m$ ,  $m \leq n$ .
13:  return  $k$ 
14: procedure ENCRYPTIONDECRYPTION( $m, k$ )
15:  Ensure  $|k| = |m| = n$ .
16:  Compute ciphertext  $c = m \oplus k$ 
17:  Transmit  $c$  to receiver.
18:  At receiver, decrypt  $m' = c \oplus k$ .
19:  return  $c, m'$ 

```

secret key to match the message for encryption, we obtain encrypted weights $E = e_1 e_2 \dots e_n$ by

$$E = (e_i)_{i=1}^n$$

where, $e_i = f(m_i, k_i) = \text{chr}(\text{ord}(m_i) + 2 * \text{ord}(k_i) \bmod 256)$, $\text{ord}(x)$ is the unicode point of character x (0-127 for ASCII characters) using the encoding function f and the operation of the mod ensures the range $[0, 255]$. It is experimentally depicted in Figure 5. To decrypt the message, we reverse the encryption procedure using $f(e_i, k_i) = \text{chr}(\text{ord}(e_i) - 2 * \text{ord}(k_i) \bmod 256)$ to encode the message character e .

Let $\theta \in \mathbb{R}^d$ be the input parameter vector with d elements, $\epsilon > 0$ be the privacy budget, $S > 0$ be the sensitivity, then noise scale.

$$b = \frac{S}{\epsilon}.$$

The noise vector $N \in \mathbb{R}^d$ is generated element-wise as follows:

- For the Laplace mechanism, $N_i = \text{Laplace}(0, b, \text{size} = \theta.\text{shape})$.
- For the Gaussian mechanism, $N_i \sim \mathcal{N}(0, \sigma^2)$, $\forall i = 1, \dots, d$. where $\sigma = \sqrt{2 \ln \left(\frac{1.25}{\delta} \right)} \cdot b$.

Finally noisy params,

$$\theta' = \max(\theta + N, 0)$$

QFL is in some way similar to classical FL in that clients and devices train locally with their dataset collaboratively and contribute to the global model while keeping the data private at the local device. However, there are multiple aspects of the QFL setup. QFL has some peculiar features different from the classical approach of learning. First, we need to encode the

classical dataset into a quantum representation. The main goal with the federated averaging version of QFL is such that

$$\min_{\theta} \sum_{k=1}^K \frac{n_k}{n} \mathcal{L}_k(\theta)$$

where, $\mathcal{L}_k(\theta)$ is the local loss in client k using its parameterized quantum circuit, n_k is the number of samples in client k as $n = \sum_{k=1}^K n_k$. Whereas, at each local client evaluates a quantum loss function using a parameterized quantum circuit $U(\theta)$ as,

$$\mathcal{L}_k(\theta) = \mathbb{E}_{x \sim \mathcal{D}_k} [\ell(f_{\theta}(x), y)]$$

where, $f_{\theta}(x)$ is the output of the quantum model (eg. expectation value from quantum measurement) and ℓ is a classical loss function (like MSE or cross-entropy). For parameter aggregation, we have the following.

$$\theta^{(t+1)} = \sum_{k=1}^K \frac{n_k}{n} \theta_k^{(t)}$$

where, $\theta_k^{(t)}$ is the locally trained parameter at round t on client k .

The following steps are carried out in the proposed framework. Suppose that we have model weights as a vector $\theta \in \mathbb{R}^n$ where $\theta = (a_1, a_2, \dots, a_n)$. For DP, we produce a perturbed version θ' by adding a noise vector $\eta \in \mathbb{R}^n$ as,

$$\theta' = \theta + \eta$$

Two popular approaches used for the choice of the noise distribution for η are the Laplace mechanism (for ϵ -DP) and the Gaussian mechanism for (ϵ, δ) -DP. With the Laplace mechanism, we have

$$\Delta_1 = \max \|\theta - \theta'\|_1$$

where, Δ_1 is the l_1 sensitivity of the weights, i.e., the maximum l_1 norm bound on how much θ can vary under perturbations. Each component n_i (for $i=1$ to n) is drawn independently from a Laplace distribution as,

$$\eta_i \sim \text{Lap}(0, \frac{\Delta_1}{\epsilon})$$

such that

$$p(x|0, b) = \frac{1}{2b} \exp\left(-\frac{|x|}{b}\right),$$

with scale $b = \frac{\Delta_1}{\epsilon}$

With Gaussian mechanism, suppose that Δ_2 is the l_2 sensitivity of the weights, i.e. the maximum l_2 norm bound on variables in θ as,

$$\Delta_2 = \max \|\theta - \theta'\|_2.$$

Then, the noise vector is multivariate Gaussian as

$$\eta \sim \mathcal{N}(0, \sigma^2 I_n)$$

with variance calibrated as,

$$\sigma \geq \frac{\Delta_2 \sqrt{2 \ln(1.25/\delta)}}{\epsilon}$$

Let $\theta \in \mathbb{R}_{\geq 0}^d$ denote the vector of model parameters, where d is the dimension corresponding to the flattened shape of the input array *params*. Let Δ be the sensitivity parameter, $\epsilon > 0$ be the privacy budget, $m \in \{\text{laplace}, \text{gaussian}\}$ be the noise mechanism, and δ be the *decimals* be the number of decimals for rounding. Then, operation on the model parameters can be summed as

$$\tilde{\theta} = R_\delta \circ C_0(\theta + \eta),$$

where, $\eta \in \mathbb{R}^d$ is the noise vector, $C_0 : \mathbb{R}^d \rightarrow \mathbb{R}_{\geq 0}^d$ is the component wise clipping operator such that $[C_0(x)]_i = \max(x_i, 0)$ for $i = 1, \dots, d$. $R_\delta : \mathbb{R} \rightarrow \mathbb{R}^d$ is the component wise rounding operator to *decimal* places.

Assuming Δ is chosen appropriately, as the sensitivity of the parameters θ , the mechanisms provide differential privacy. Both the mechanism with or without clipping and rounding preserves the privacy of DP. Since clipping is a deterministic, data-independent function that maps to the non-negative, and rounding introduces quantization which is also similar but with finite-precision arithmetic, rounding can slightly amplify the effective privacy loss

QKD enables two parties to share cryptographic keys with provable security, even when the quantum communication channel is potentially insecure [30]. Building on this, we extend the unconditional security proof of the BB84 QKD protocol to cover any arbitrary attack permitted by quantum mechanics, under the assumption that the eavesdropper possesses unbounded computational resources and full quantum capabilities, as formulated in [31]. From [31], assumptions for the security proof of QKD include:

Assumption III.1 (Secure Classical Channel). *The client and server share a classical communication channel that is immune to jamming or is authenticated using a short, pre-shared secret key.*

The classical channel cannot be jammed or disrupted by an adversary, ensures messages sent over the classical channel are genuine and not tampered with.

Assumption III.2 (Adversary Limitations). *The adversary can attack the quantum channel and eavesdrop on all classical channel communications but cannot compromise the security of the client's or server's laboratories.*

This means that the adversary can attack the quantum communication channel and passively listen to all communication on the classical channel, but the physical setup and devices (where quantum states are prepared) of the client and the server are secure.

Assumption III.3 (Qubit-Based Communication). *The sender transmits quantum information using qubits, which are two-state quantum systems.*

Transmitting information using qubits which are quantum systems with two possible states.

Assumption III.4 (Unlimited Adversary Technology). *The adversary has access to unlimited quantum technology, including quantum memory and quantum computing capabilities.*

This assumption states that the adversary has access to unlimited quantum technological resources, including memory and quantum computers.

In the BB84 protocol, the sender and recipient use four possible quantum states, known as BB84 states, distributed over three distinct bases. This includes employing the “spin” notation and its association with the “computational basis” notation as $|0_z\rangle = |0\rangle$, $|1_z\rangle = |1\rangle$, $|0_x\rangle = \frac{1}{\sqrt{2}}(|0\rangle + |1\rangle)$ and $|1_x\rangle = \frac{1}{\sqrt{2}}(|0\rangle - |1\rangle)$.

In this context, after the sender has transmitted states and compared bases, a shared key is produced if both the sender and receiver utilize the same basis. Following this, a shifted key is established which is subsequently used to formulate the final key.

To model the potential threat, we can have general attack, sequential attack, etc. With general attack, an adversary may attack qubits by initially executing a unitary transformation on both the sender's qubit and its probe. This probe is retained in memory and utilized only once all classical data, including bases of all bits, choices of test bits, and test bit values, are obtained from both the sender and receiver. Using this information, an optimal measurement is carried out on the probe to extract as much information as possible about the resulting secret key. For Q_i quantum systems that send the sender to the receiver, Adversary may coherently intercept all n systems and apply an arbitrary quantum channel $\mathcal{A} : Q^n \rightarrow EQ^n$ (General Attack), subsequently forwarding the Q^n output systems (n quantum systems) to the legitimate receiver [32]. With the following assumption,

Assumption III.5 (Single Quantum System Constraint). *The adversary can possess only one quantum system Q_i at a time.*

This implies that the adversary cannot simultaneously hold or manipulate multiple quantum systems during the attack on the quantum communication channel.

Regarding a sequential attack strategy, the sender dispatches the systems Q_1, Q_2, \dots, Q_n in a specific sequence, necessitating that adversary's attack also follow the same sequence. Consequently, the attack is characterized by a series of mappings $A_i : E'_{i-1}Q_i \rightarrow E'_iQ_i$, where E'_{i-1} represents the adversary's knowledge prior to interacting with Q_i , E'_i denotes her updated information post-processing of Q_i , and Q_i is forwarded to the receiver after the adversary's intervention.

For vQFL setting with N clients, T communication rounds, the full attack can be given by the tensor product map,

$$\mathcal{A}^{\otimes n} : Q^n \rightarrow EQ^n \quad \forall N, T$$

The security and robustness of QKD can be examined in more detail as follows. Conditioned on passing the test, adversary's information about sender's key becomes exponentially small, such as

$$I(A; E | T = \text{pass}) < A_{\text{info}} e^{-\beta_{\text{info}} n}$$

where, $I(A; E | T = \text{pass})$ denotes the mutual information between the sender's key A and the adversary's knowledge E , conditioned on the event that the test is passed, and n represents the number of qubits used in the protocol. However,

this condition is not satisfied in the presence of attacks such as the SWAP attack. Similarly, it also fails under a half-SWAP attack, in which the adversary, with probability $\frac{1}{2}$, leaves the sender's qubit unchanged so that it reaches the receiver without disturbance, causing the test at the receiver's end to pass with high probability. With the remaining half of the probability, adversary executes a SWAP attack: it intercepts the qubits sent by sender, transmits randomly prepared states to receiver instead, and only later performs measurements on sender's original qubits. So, on average, $I(A; \varepsilon) = \frac{m}{2}$ and $P(T = \text{pass}) \geq \frac{1}{2}$.

Accordingly, the appropriate security requirement should bound the joint probability that both undesirable events occur simultaneously: namely, that adversary obtains non-negligible information ($I_{\text{adversary}} \geq A_{\text{info}} e^{-\beta_{\text{info}} n}$) and that the protocol still passes the test ($T = \text{pass}$). Thus, the security criterion is [31]:

$$P[(T = \text{pass}) \wedge (I_{\text{adversary}} \geq A_{\text{info}} e^{-\beta_{\text{info}} n})] < A_{\text{luck}} e^{-\beta_{\text{luck}} n}$$

where, T denotes the outcome of the test and $I_{\text{adversary}} = I(A; E | i_T, C_T, b, s)$ represents the amount of information adversary possesses about the key, given the protocol parameters (i_T, j_T, b, s) that are revealed by sender and receiver. The test is considered passed when $C_T = i_T \sim j_T$ satisfies $|C_T| \leq n_{\text{allowed}}$. Sender and receiver can enhance security by choosing a larger number of bits n . In that case, the probability that the protocol both passes the verification test and leaves adversary with substantial information decreases exponentially. Moreover, regarding reliability, the likelihood that the final keys held by each client and the Server disagree is exponentially small, namely

$$P(A \neq B) \leq A_{\text{rel}} e^{-B_{\text{rel}} n}$$

The most general strategy available to adversary is to couple an ancillary quantum probe to the transmitted qubits, apply a global unitary operation U on the combined system of all qubits and her probe, and then forward the resulting, potentially disturbed, qubits on to the receiver. Subsequently, once the sender and receiver have disclosed all classical information, it performs the optimal measurement on her probe. The unitary operator U is expressed as follows.

$$U(|0\rangle|i\rangle) = \sum_j |E'_{i,j}\rangle|j\rangle$$

where, $|E'_{i,j}\rangle$ denote the states of adversary's probes when the sender transmits $|i\rangle$ and the receiver obtains $|j\rangle$, i is a bit string that the sender encodes using a chosen base set b , and the receiver measures a string j in the same bases; $|0\rangle$ represents a probe initialized by an adversary in some unknown state.

For QKD to be secure, it satisfies the following:

- 1) **Correctness:** If the protocol does not abort, the sender's key K and the receiver's key K' are equal with high probability, such that

$$\Pr[K \neq K' | \text{no abort}] \leq \varepsilon_{\text{cor}}.$$

The probability of the keys being different, since the protocol does not abort, is bounded by a small error term

ε_{cor} . This accounts for the robustness against adversarial interference that might cause discrepancies between keys.

- 2) **Secrecy:** The adversary's knowledge of the final key is negligible, with the trace norm distance between the actual state $\rho_{KE|\Omega}$ (conditioned on no abort) and the ideal state $\tau_K \otimes \rho_{E|\Omega}$, where τ_K is the maximum mixed state in the system K and Ω is the event without abort, bounded by a small error term ε_{sec}

$$\|\rho_{KE|\Omega} - \tau_K \otimes \rho_{E|\Omega}\|_1 \leq \varepsilon_{\text{sec}}.$$

This property guarantees that the adversary gains negligible information about the final key. Secrecy is quantified by comparing the actual quantum state of the key and adversary's system ($\rho_{KE|\Omega}$, conditioned on the protocol not aborting) to an ideal state where the key is maximally mixed ($\tau_K \otimes \rho_{E|\Omega}$).

- 3) **Completeness:** For a given noise model, there exists an honest adversary behavior such that the protocol aborts with a probability that is small bounded by $\varepsilon_{\text{comp}}$ as

$$\Pr[\text{abort}] \leq \varepsilon_{\text{comp}}.$$

This property ensures that the protocol is robust against noise in the communication channel. This also ensures that the protocol is practical and is likely to succeed under realistic conditions.

Thus, the QKD protocol is $(\varepsilon_{\text{cor}} + \varepsilon_{\text{sec}}/2)$ -secure.

IV. EXPERIMENTAL ANALYSIS

This section highlights the method we used to prepare the datasets, define our analysis metrics, and various results, including ablation studies.

A. Datasets.

In terms of dataset, we utilize three state-of-the-art datasets: Waymo dataset¹, KITTI dataset² and nuScenes³ dataset.

KITTI. This dataset comprises a collection of vision tasks developed using an autonomous driving platform. It includes an object detection dataset featuring monocular images and bounding boxes, with 7,481 training images annotated with 3D bounding boxes. It is an autonomous driving dataset developed by the Karlsruhe Institute of Technology, Germany, and Toyota Technological Institute at Chicago, USA [33]. We utilized TensorFlow Datasets to extract/download the dataset. Object type labels are Car, Van, Truck, Pedestrian, Person_sitting, Cyclist, Tram, and Misc which are represented from numbers 0 to 7. Bounded boxes and labels are extracted with a specific batch size. The complete data set contains both both train set (6347), the test set (711), and the validation set (423). We extract small 64 x 64 grayscale image patches (cropped) from every annotated object detected in every image. The other steps involved normalizing the bounding box into real pixel coordinates, cropping the object tightly from left camera image, resizing to 64 x 64 pixels using smooth bilinear resizing

¹<https://github.com/waymo-research/waymo-open-dataset>

²<https://www.cvlibs.net/datasets/kitti/>

³<https://github.com/nutonomy/nuscenes-devkit>

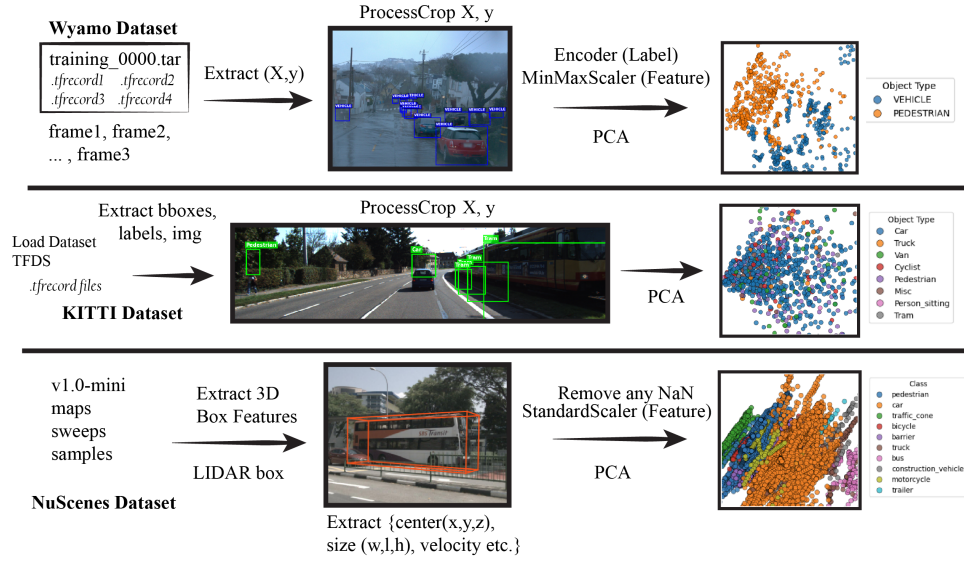


Fig. 6: These SOTA datasets are huge and challenging to process. A brief process use to perform experimental analysis is shown for all datasets - Waymo, KITTI and nuScenes.

which are converted to grayscale, flattened into 4096 length vector and the patches saved with their class names. The train dataset is distributed among the devices while the test dataset is used for the server device. We follow the StandardScaler or MinMaxScaler and PCA transformation with label encoding applied in some cases, as shown in Figure 6. After crop patching, we have 33414 patches for training and 3197 patches for validation. However, we only take a small sample of randomized dataset samples for our experimental analysis, such as 2000 samples distributed among training devices, while 100 samples for server test. In terms of label distribution, we can observe in Figure 7d that there is a class imbalance between label (0) which is “car” and others. Figures 7a and 7b show sample images with bounding boxes and Figure 7c shows 100 samples with the first components after PCA implementation.

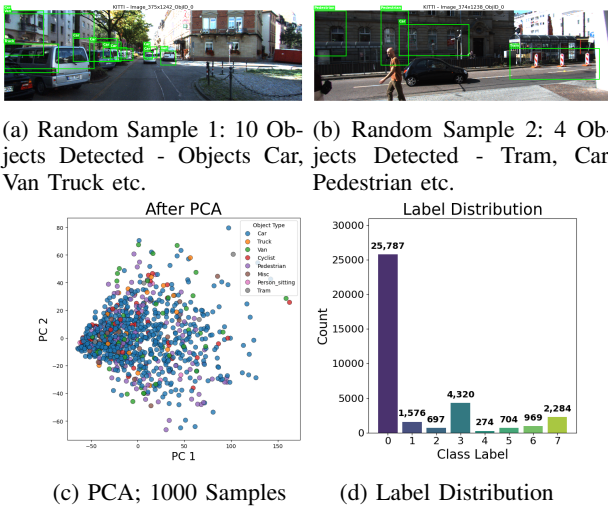


Fig. 7: KITTI Dataset: (a, b) Sample images with bounding boxes, (c) PCA figure and (d) Label Distribution.

Waymo. Waymo Open Dataset is a large-scale, high quality diverse dataset consisting of 1150 scenes that each span 20 seconds [34]. The data captured across a range of urban and suburban geographies are well synchronized and high quality calibrated LiDAR and camera data exhaustively annotated with 2D (camera image) and 3D (LiDAR) bounding boxes providing strong baseline for 2D and 3D detection and tracking masks. Figures 8a and Figure 8b show visualization for objects in frames 0 and 77, respectively, which is in the scene of Waymo dataset TFRecord file from training_000.tar file, specially focusing on front camera images and drawing 2D bounding boxes around the detected objects. The object types selected are vehicle, pedestrian and cyclist for visualization, which is present in a single TFRecord file extracted from a Waymo training dataset. To process the dataset, we first load one TFRecord archived in .tar files, which reads one segment file containing multiple frames. Each sample is an entire front image that is cropped for objects that are flattened, and each label is one type of object. We used only small samples for our experimental analysis. Waymo and KITTI data experiments were performed in the wsl windows environment using a local jupyter notebook, while others (also KITTI and nuScenes) were performed in the Google colab environment. Figures 8d, 8c and 8e show the plot of PCA components 100, all sample and label distribution, respectively. As we can observe, from that particular .tar file, we have more label 2 samples while almost very low 0 label classes, as seen in Figure 8e.

nuScenes. The nuScenes dataset consists of various scenes with 23 categories, 8 attributes, 12 sensors, etc. [12]. We utilized the v1.0-mini version of the dataset, which has 10 scenes within which there are 404 samples containing additional sample data and annotations. There are various scenes within the dataset such as scene-0061 that contains parked truck, construction, etc. while scene-0103 contains many vehicles right, waiting for the car, etc. Each sample data set contains data from RADAR_FRONT, RADAR_FRONT_LEFT,

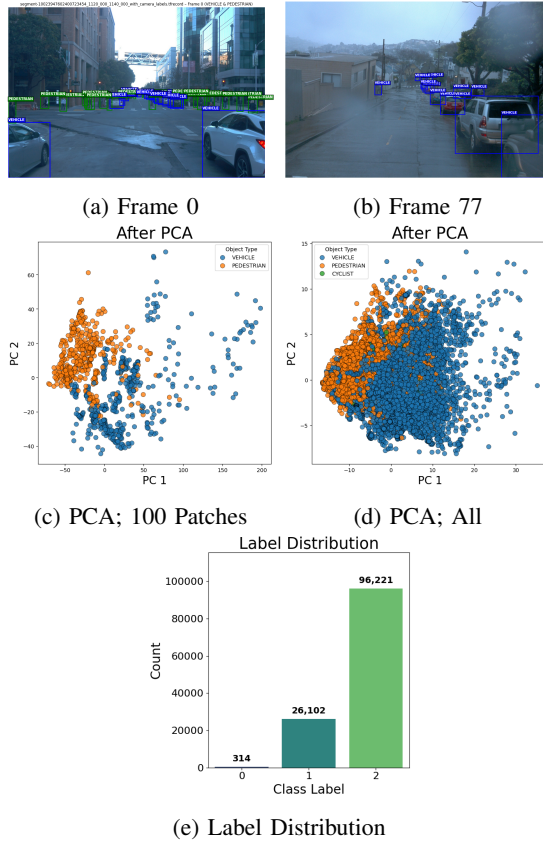


Fig. 8: Waymo Dataset: (a, b) Sample images, (c, d) PCA 100/full, (e) Label distribution in that sample of the dataset.

LIDAR_TOP, etc. A sample CAM_FRONT scene is shown in Figure 9a which shows various vehicle types with their bounding boxes. To extract features and labels, we first localize nuScenes data v1.0-mini. Then, class mapping is either done to convert to numerical labels or keep the categorical labels as it is. Then, we extract 3D box features for every annotation in every sample. The LIDAR box is retrieved via `get_sample_data()`. The extracted features are center (x,y,z), size (w,l,h), yaw, velocity(vx, vy, vz), num_lidar_points. Also, we remove any NaN rows, which is followed by StandardScaler/MinMaxScaler, PCA and train test split methods. For this dataset, we extract input features from boxes for each annotation, which consists of 'xyz: [x, y, z]' location, dimensions 'wlh: [w, l, h]', orientation, velocity, and number of lidar points. For each annotation, we assign a category such as 'human.pedestrian.adult', 'vehicle.bicycle' etc. as in Table II which we converted into their numerical representation from 0 to 9 for barrier:0 to truck:9 (in some categorical labels were not changed). Once we extract all the annotation features and remove any 'nan' values, we have altogether 185,080 samples of input feature matrix with their corresponding labels. We also apply a test with PCA to reduce from 11 features to 4 feature dimensions and in some cases discard certain features and keep only 7 features and perform no PCA. And also, experiment with all samples along with small sample of 1000 training samples distributed among 10 devices with 100 samples for server device for testing.

Figures 9a and 9b show the sample images while Figures 9c, 9d and 9e show PCA component plots with scalars used StandardScaler, MinMaxScaler or no Scaler, respectively. In Figure 9f we show the number of labels with all labels and in Figure 9g, we select only a few labels and show in the pie chart. The label class imbalance seems to be the issue while training due to which there were performance issues with the full dataset for nuScenes.

TABLE II: nuScenes class mapping; Only few classes used for some experiments

Original Class	Mapped Class
movable_object.barrier	barrier
vehicle.bicycle	bicycle
vehicle.bus.bendy	bus
vehicle.bus.rigid	bus
vehicle.car	car
vehicle.construction	construction_vehicle
vehicle.motorcycle	motorcycle
human.pedestrian.adult	pedestrian
human.pedestrian.child	pedestrian
human.pedestrian.construction_worker	pedestrian
human.pedestrian.police_officer	pedestrian
movable_object.trafficcone	traffic_cone
vehicle.trailer	trailer
vehicle.truck	truck

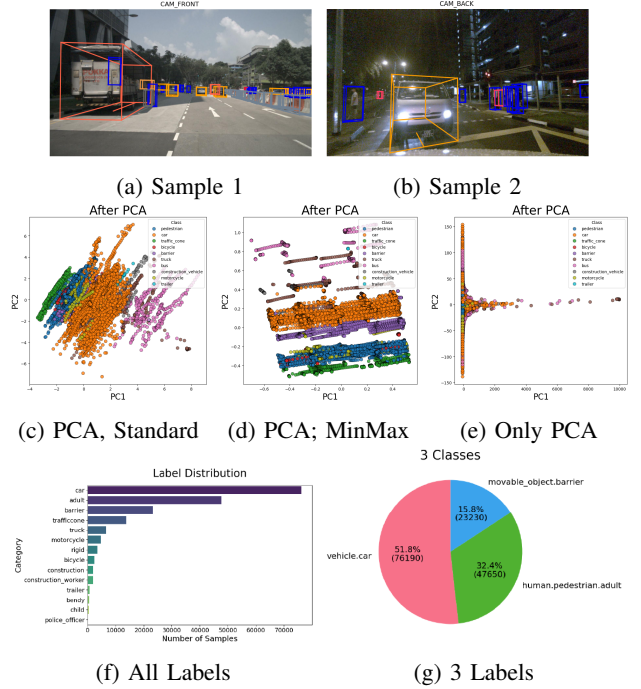


Fig. 9: nuScenes Dataset v1.0-mini CAM FRONT: (a, b) samples of a scene which multiple objects and their bounding boxes with annotations; v1.0-mini, (c, d, e) Effect of PCA with standarScaler, MinMaxScaler or with no Scaler; (f) Label Distribution, (g) Only some selected label distribution.

B. Tools & Metrics

In terms of a quantum machine learning tool, we utilize the Qiskit library. Within Qiskit library, we utilize Quantum Convolutional Neural Network (QCNN), Variational Quantum Classifier (VQC) and SamplerQNN with Network Classifier. The metrics for analysis are accuracy at the server and device level, the objective values of the local optimizer functions, and the total communication time required to complete each communication round, as also shown in Figure 10.

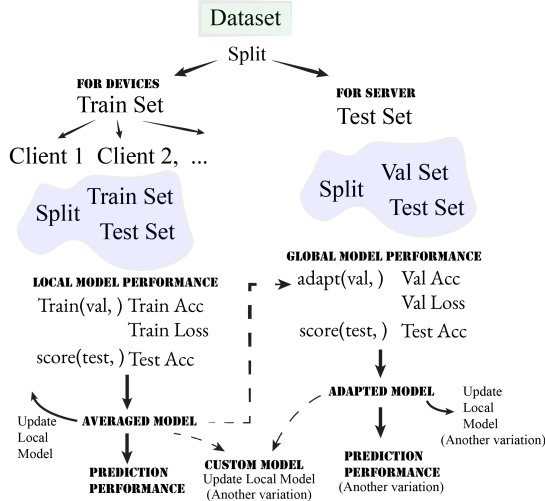


Fig. 10: Data Split, Metrics Definition etc - The methods used to prepare datasets, define metrics and results in our work.

- **Global FineTuned (FT) Model Performance:** Global Model FT Test Accuracy, Validation Loss, and Validation Accuracy - These metrics are computed on the server device, which has a set of validation and test set dataset. Once we obtain the global average model, we validate it against the server dataset. Here, we learn how capable the average global model is of optimizing or learning on the validation set and performing on the test set again. This is still fitting the average model on the validation set of the server which follows same optimization steps as in training in local model devices. Depending upon the ablation study, this fine tuned model is only used for performance analysis and not to update devices local model unless mentioned otherwise in this work.
- **Local Model Performance:** Test Accuracy, Train Accuracy, Train Loss, Train Time - Each device has their own train set and test set dataset as well. Training accuracy tests how well the device model is able to learn with each new updated average model parameter, which also computes the train loss. Whereas, test accuracy is performance of newly trained local model before sending to server on test set at local device.
- **Global Prediction Model Performance:** Prediction test accuracy, validation accuracy, and prediction loss - This metric is prediction performance of a newly formed average global model or a customized/adapted global model depending upon the experiment and ablation study. The prediction validation accuracy and the loss result is in the validation set of the server data set and the prediction test result with the test set of the server dataset. We include these metrics to measure the performance of the global model in performing prediction accuracy on the dataset of the server test set. This model is different and separate from the optimized FL global model performance, and thus we term it as global prediction model.
- **Communication Time:** Communication time involves the total time required to complete one communication round.

C. Models - VQC, SamplerQNN, QCNN

We perform series of experiments to compare between various models like VQC, QCNN and NeuralNetworkClassifier with SamplerQNN with all datasets: KITTI, nuScenes, and Waymo. With the KITTI dataset, we see that the prediction model performance is better with QCNN as shown in Figures 11a, 11b and 11c for the prediction test accuracy, validation accuracy, and loss, respectively. While SamplerQNN performs worst in terms of prediction test accuracy, val accuracy, and in average device performance, as shown in Figures 11e and 11d. With communication time, QCNN seems to be faster than in Figure 11f. However, in terms of fine tuning process and performance, we see better results with VQC as shown in Figures 11g and 11h for test accuracy and validation accuracy, respectively.

With Waymo dataset, we only consider 2 classes, either vehicle or pedestrian. We can observe that in Figure 12, QCNN performs similar to VQC and better than SamplerQNN all in terms of prediction accuracy as in Figures 12a and 12b, while in Figures 12d and 12e, QCNN does not perform well in terms of average devices performance. However, VQC is observed to be slower in terms of communication time as shown in Figure 12f. As waymo was experimented within wsl environment using local jupyter notebook, running multiple jupyter notebooks in parallel might have impacted the results in terms of communication time. For fine tuned results, VQC performs overall best in both test accuracy and validation accuracy as shown in Figures 12g and 12h respectively.

With nuScenes data, VQC performs better in terms of devices, prediction, and finetuned model results, as in Figure 13. While QCNN is slowest as shown in Figure 13f. In summary, we observed QCNN performed better with KITTI dataset but not with nuScenes dataset and was similar to VQC somehow with Waymo dataset. In most cases, VQC stands out in terms of its performance in all datasets. This highlights the performance variation and capability of different models in performing various tasks, and thus correct selection of a specific model to do the work is required.

For the KITTI dataset, the experimental setup uses 2000 training samples partitioned across client devices and 100 samples reserved for server-side testing, with a maximum of 100 training iterations and 10 participating devices. For the Waymo dataset, we similarly employ 2000 training samples distributed among devices and 100 server test samples, again using a maxiter setting of 100 and 10 devices. For the nuScenes dataset, the configuration consists of 1000 training samples allocated to devices and 100 samples for server testing, with a maximum of 100 iterations and 10 devices.

Table III shows further results in detail showing other results such as average results for the global model, which is average performance in all communication rounds and final performance is the last result at the end of all communication rounds. The table also includes the top results chosen from all communication rounds for global prediction results. In brief, with the KITTI dataset, VQC performs the best in terms of accuracy, prediction while for training, we can see similar results between QCNN and VQC. Overall, VQC also performs

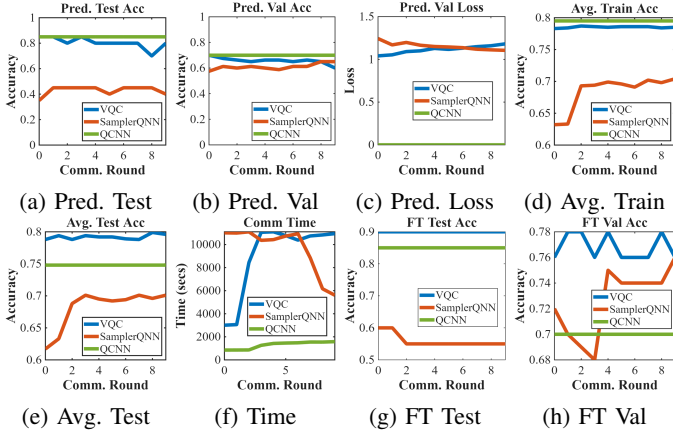


Fig. 11: Models Comparison on KITTI Dataset; Prediction Model, Fine-Tuned Model, Average Devices Performance, Communication Time

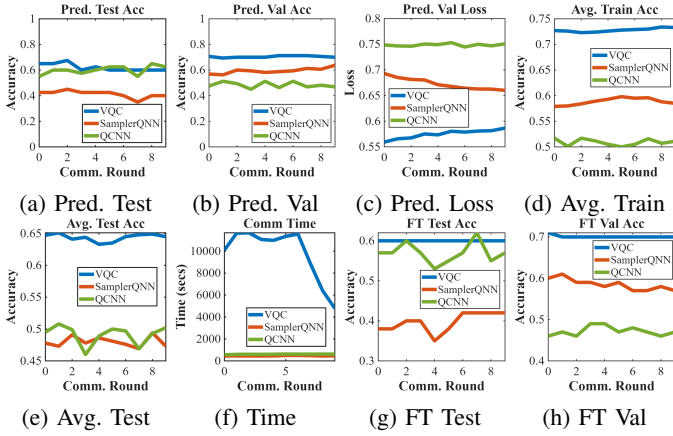


Fig. 12: Models Comparison on Waymo Dataset; Prediction Model, Fine-Tuned Model, Average Devices Performance, Communication Time

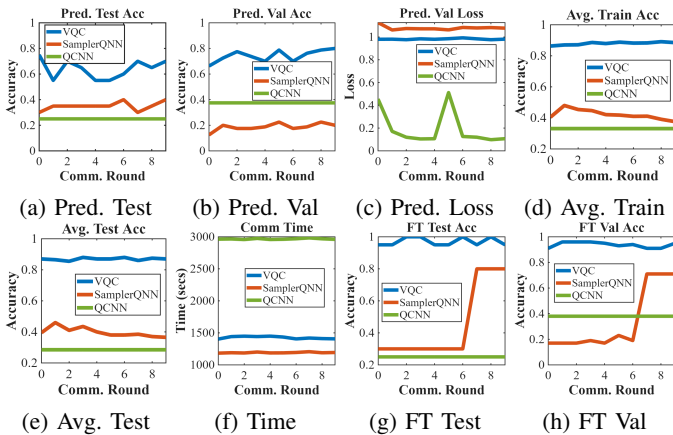


Fig. 13: Models Comparison on nuScenes Dataset; Prediction Model, Fine-Tuned Model, Average Devices Performance, Communication Time

well for the Waymo and nuScenes dataset.

D. Number of Devices - Waymo

For this experiment, we randomly extracted small set from the dataset so that each device has 50 data samples for faster computation. Then we experiment with 3, 20, 100, 200 devices and observe the performance in terms of average devices performance (Figures 14a, 14b), fine tune model test accuracy (Figure 14c) and communication time (Figure 14d). We get better results with more devices (200 D) devices in terms of average device performance with only 3 devices performing worst in terms of accuracy and FT model performance but with communication overhead as expected with a greater number of devices.

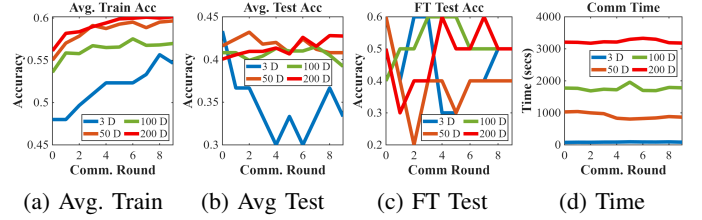


Fig. 14: Impact of number of devices: 3, 20, 100, 200 Devices

E. Learning Behaviour of Devices

We observe the behaviors of the devices as in Figure 15. We plot devices local objective values and observe that they all behave differently among 50 devices with each having 50 data samples Waymo dataset, 100 max iter for COBYLA optimizer run for 10 communication rounds. Figure 15a shows devices with low object values ranging from 1.2 to close to zero, while Figure 15b shows devices with high object values ranging from around 29 to 22 which is much poorer than the other cohort of devices. This behavior of devices could impact the overall performance of the devices, not letting global optimization reach as desired as one group of devices performs much lower than the other group of devices. Considering this Waymo dataset has max 3 classes and thus not completely representing non IID scenario, a proper investigation to this behavior of devices performing differently drastically is required and thus deferred to our future work.

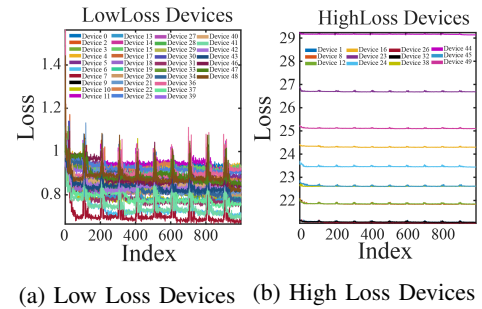


Fig. 15: Devices Behavior: Two group of devices in same vQFL set up behaving different in terms of local learning with contrasting objective values.

TABLE III: Global FT Model, Prediction Model and Local Model Performance

Dataset	Model	Global Fine-tuned Model						Local Model				Comm. Time	Global Prediction Model								
		Val Acc		Test Acc		Val Loss		Train Acc		Test Acc			Val Loss		Val Acc			Test Acc			
		Avg	Final	Avg	Final	Avg	Final	Avg	Final	Avg	Final		Avg	Final	Avg	Final	Top	Avg	Final	Top	
KITTI	VQC	0.7680	0.7600	0.9000	0.9000	1.03	0.98	0.79	0.79	0.79	0.80	9036.35	1.1147	1.1807	0.6575	0.6000	0.7000	0.8050	0.8000	0.8500	
	SamplerQNN	0.7260	0.7600	0.5600	0.5500	1.41	1.25	0.68	0.70	0.68	0.70	9618.97	1.1541	1.1053	0.6113	0.6500	0.6500	0.4300	0.4000	0.4500	
	QCNN	0.7000	0.7000	0.8500	0.8500	1.23	0.87	0.80	0.80	0.75	0.75	1287.69	0.0000	0.0000	0.7000	0.7000	0.7000	0.8500	0.8500	0.8500	
Waymo	VQC	0.7010	0.7000	0.6000	0.6000	0.8035	0.7886	0.73	0.73	0.64	0.65	9841.01	0.5749	0.5866	0.7044	0.7000	0.7125	0.6200	0.6000	0.6750	
	SamplerQNN	0.5850	0.5700	0.3970	0.4200	0.4433	0.4353	0.59	0.58	0.48	0.47	462.12	0.6728	0.6601	0.5944	0.6375	0.6375	0.4125	0.4000	0.4500	
	QCNN	0.4720	0.4700	0.5700	0.5700	1.0814	1.0786	0.51	0.51	0.49	0.50	606.16	0.7486	0.7508	0.4838	0.4688	0.5125	0.6000	0.6250	0.6500	
nuScenes	VQC	0.9380	0.9500	0.9700	0.9500	1.0819	1.0124	0.88	0.89	0.87	0.87	1426.26	0.9824	0.9815	0.7438	0.8000	0.8000	0.6400	0.7000	0.7500	
	SamplerQNN	0.3420	0.7100	0.4500	0.8000	0.9944	0.8036	0.42	0.38	0.40	0.36	1191.79	1.0797	1.0781	0.1875	0.2000	0.2250	0.3500	0.4000	0.4000	
	QCNN	0.3800	0.3800	0.2500	0.2500	0.4534	0.4142	0.33	0.33	0.29	0.29	2966.30	0.1920	0.1070	0.3750	0.3750	0.3750	0.2500	0.2500	0.2500	

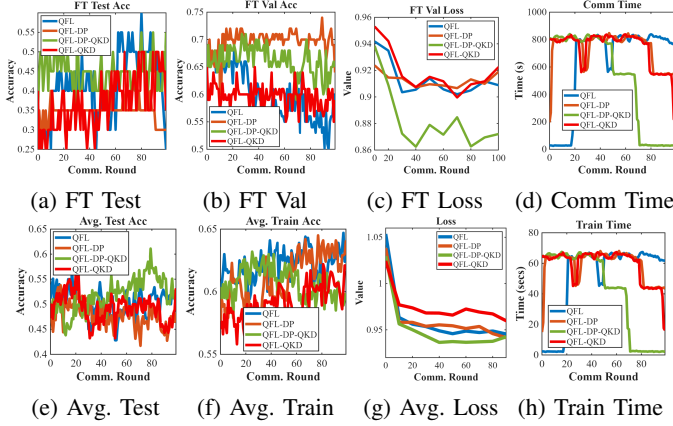


Fig. 16: Model Performance: Waymo Dataset; QFL, QFL-DP, QFL-QKD, QFL-DP-QKD

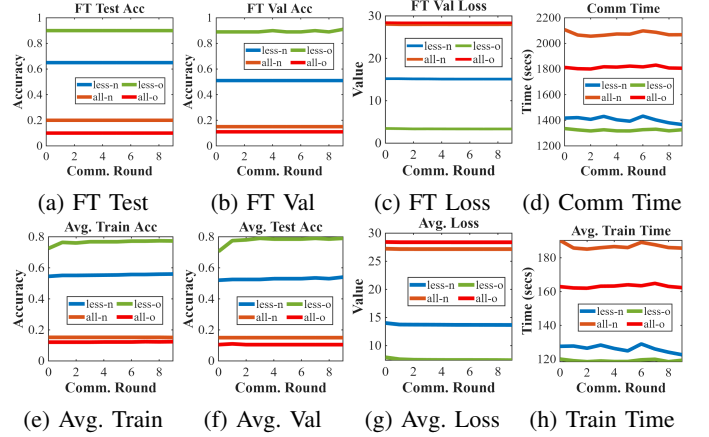


Fig. 17: Model Performance: nuScenes Less Dataset

F. Results - DP, QKD

These are additional results that are compared to see if there was any impact on standard QFL due to QKD, DP integration, etc. The experiment is performed with the methods QFL, QFL-DP, QFL-QKD and QFL-DP-QKD representing default QFL, QFL with differential privacy, QFL with QKD implementation, and final QFL with both DP and QKD implemented. In Figure 16, we observe the performance (FT model) of the server device with the Waymo dataset which was run for 100 communication rounds with 1000 train samples distributed among 10 devices with optimizer 10 maxiter. In terms of validation accuracy and test accuracy, as in Figures 16a and 16b, QFL-DP-QKD and QFL-DP perform better than other methods, respectively. However, as seen in Figure 16c, in terms of the loss values of the objective function, QFL-DP-QKD performs better. In terms of device performance, devices perform best on average validation accuracy with QFL-DP-QKD as in Figure 16e and on average train accuracy with QFL and QFL-DP as in Figure 16f. In terms of training time per device and overall communication round, with added DP and QKD implementation, there is no impact as expected. However, real implementation of QKD can be far more complex than one implemented in this study for proof-of-concept. Also, the pattern is similar in terms of average devices training time (Figure 16h and total communication round time 16d which implies that most of the difference in communication overhead is similar other than each individual device training time.

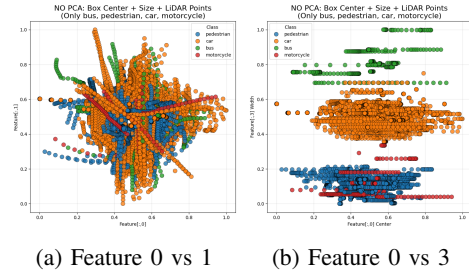


Fig. 18: nuScenes Less Features and No PCA

G. Nuscenes Dataset - Less Features.

In nuScenes dataset, we have altogether 11 features extracted including xyz, wlh, lidar points, rotation angle, etc. with all the labels as default such as pedestrian, car, truck, etc. But in this experiment, we have selected a few features of 7 and also reduced labels to car, truck, and pedestrian. We did not apply PCA in these experiments and used all features, which implies an equal number of qubits (7 features) used in the circuits. From the results in Figure 17, we can observe improved performance with fewer features and labels. We compare between less-o against all-o and less-n against all-n where “less” means fewer features (7) and “all” means all features (11) whereas “o” (old approach) and “n” (new approach) refer to slightly different ways of processing data, but still with most similarity and are mentioned just so they can be compared correctly. In all aspects, less-o performs better in terms of server test accuracy as in Figure 17a, validation accuracy as in Figure 17b, server validation loss 17c and in

device performance train accuracy, validation accuracy and average loss as in Figure 17e, 17f and 17g respectively. This implies that, for VQC classifier, less number of classes is more favorable, as well as for nuScenes dataset, possibly not all features are relevant to the class labels which at least are observed in our experimental analysis. The plot between features 0 and 1 and features 0 and 3 is shown in Figures 18a and 18b respectively without applying PCA analysis.

H. Impact of class imbalance

In this section, we study the impact of class balance and imbalance. Figure 19a shows all three labels found in the selected .tar file we are using for this experiment. In Figures 19b and 19c, we observe a balanced and unbalanced number of classes, respectively. Imbalance labels are by default present in the dataset, while the balanced label is the one we prepared to study the impact. During the processing of the dataset, most of the labels are imbalanced in all datasets, with the main one label having a dominance. We observe the impact of balanced and unbalanced in Figures 20 and 21. In terms of prediction results, results from the FT model, the results are better with balanced class labels as in Figures 20a, 20b, 20c, 20d, 20f, 20e. It clearly shows the impact of an imbalanced class balance within the dataset. However, in terms of device performance, performance is still better with an unbalanced data set as in Figures 21a and 21b. This contrast result against the FT model or prediction performance shows that, in fact, within the device itself, training and testing may not have been impacted by overall distribution labels across the datasets. However, the best results in each communication round are slightly similar to both average test accuracy and the average train accuracy.

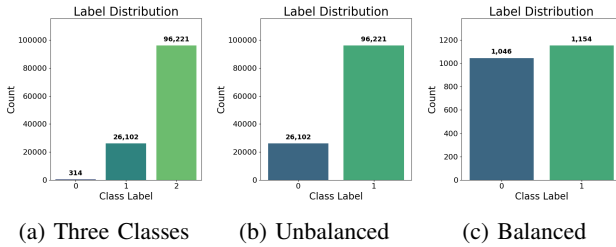


Fig. 19: Waymo Dataset: Class label distribution

I. Server Side Optimization (FT) Results

In this result, we compare three results.

- 1) No server side optimization (No FT): In this case, we train local models, average a global model. This average model is used to update local devices. After that, we first use this global model to see how well it can optimize on the server validation set and then test on the test set. This optimization and testing has no effect on device local models and is not used for prediction accuracy and loss.
- 2) Server side optimization (FT): In this case, after we create the model, we check how well it optimizes on the server validation set and then test on the test set. This optimization result, the optimized global model is used

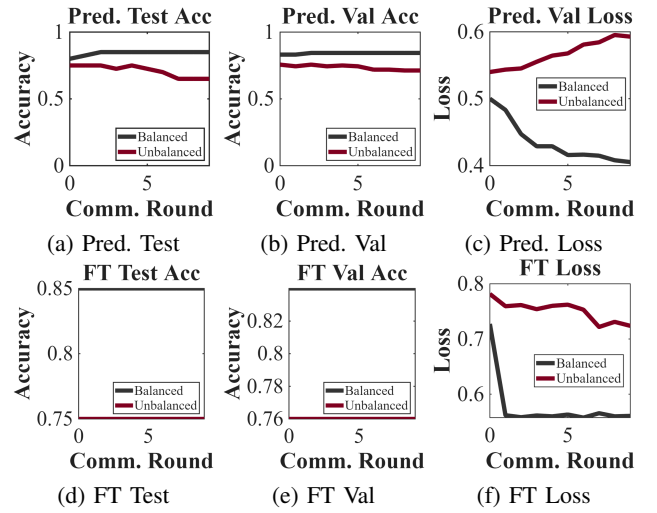


Fig. 20: Waymo Dataset: Global FT and Prediction Results

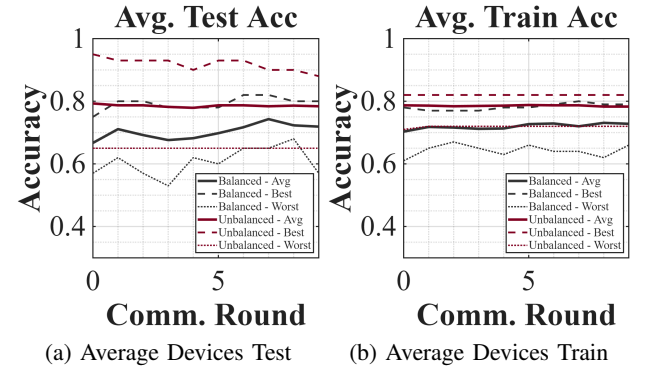


Fig. 21: Average Devices Performance: Best, Worst and Average Results

by local devices to update their local model and is also used for the prediction accuracy and loss.

- 3) Server side optimization and averaging (FT+Avg): In addition to the second step (FT), before sending optimized model to the local devices and using it for prediction accuracy, we further average this optimized model with untouched global average model developed in that communication round.

The results are device local model performance, FT global model performance, and prediction test results. The experiment was on balanced labels on the waymo dataset with only two labels (Vehicle and Pedestrian - 33,115 label 1, 26,102 label 0) as in Figure 19c. However, we only randomly take 2000 for training and 200 for test samples.

In Figure 22, we can observe that in general FT-Avg performs the best in the test accuracy of the average devices, the training accuracy, and the average training loss as in Figures 22g, 22h and 22i, respectively. This shows that fine tuning along with also considering the average model created on which the optimization or fine tuning was done, the performance is well improved in local level also. However, in terms of server performance, FT performs better than others while default No FT performs the least among the methods, as

shown in Figures 22b and 22c for server test accuracy and loss, respectively. This highlights the need for further study on how to maintain balance between the created global model and the fine tuned global model to perform optimally on both server and device levels. However, both FT and FT-Avg perform better than No FT. Thus, it highlights that FedAvg might benefit from some mechanism of fine tuning or optimization at the server side to improve overall performance at both the local and device level.

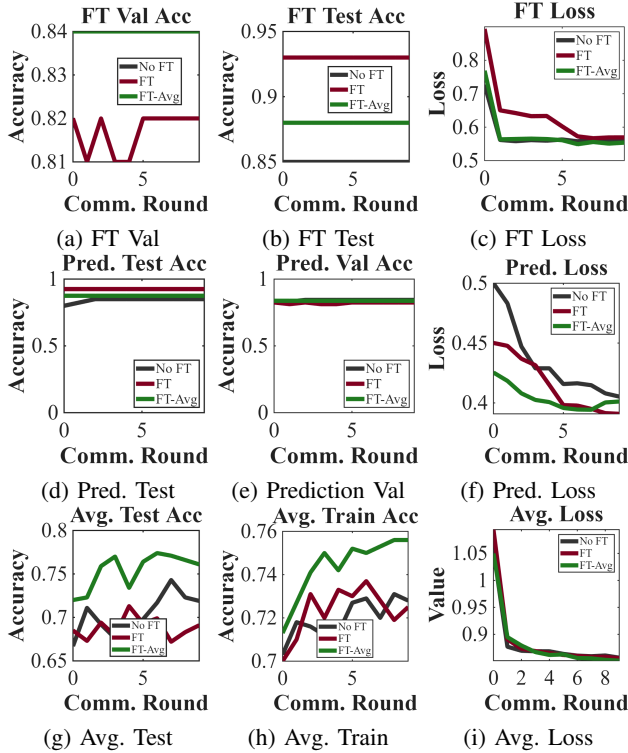


Fig. 22: Server Side Optimization (Fine tuning/Adaptation) results on Waymo dataset; FT Model performance, local model performance and prediction results.

V. CONCLUSION

In this work, we proposed a novel QFL framework for autonomous vehicles, performed study of various datasets like Waymo, nuScenes, KITTI with various quantum models like QCNN, VQC etc. In addition to the default QFL framework, we proposed a private and quantum secure vehicular QFL framework which is provable DP private providing security against model inversion and QKD integration providing further quantum security with encryption and decrypted communication channel. Further, we provide an optimized version of vQFL where we adapt the global model on the server side to improve the performance both at the local and global level. We believe that our work presents a crucial foundation for future work towards robust, reliable, and secure autonomous vehicle systems for the field of QFL. In the future, our aim is to expand our work further in tasks other than object detection such as route planning, lane detection, and semantic segmentation exploring other crucial decision-making aspects of autonomous driving in various traffic scenarios.

ACKNOWLEDGMENTS

This research was supported by an Australian Government Research Training Program (RTP) Scholarship.

REFERENCES

- [1] V. P. Chellapandi, L. Yuan, C. G. Brinton, S. H. Zak, and Z. Wang, "Federated Learning for Connected and Automated Vehicles: A Survey of Existing Approaches and Challenges," *IEEE Transactions on Intelligent Vehicles*, vol. 9, no. 1, pp. 119–137, Jan. 2024.
- [2] S. R. Pokhrel and J. Choi, "Federated Learning With Blockchain for Autonomous Vehicles: Analysis and Design Challenges," *IEEE Transactions on Communications*, vol. 68, no. 8, pp. 4734–4746, Aug. 2020.
- [3] M. Martínez-Díaz and F. Soriguera, "Autonomous vehicles: Theoretical and practical challenges," *Transportation Research Procedia*, vol. 33, pp. 275–282, 2018.
- [4] S. Y.-C. Chen and S. Yoo, "Introduction to quantum federated machine learning," in *Federated Learning*. Elsevier, 2024, pp. 311–328. [Online]. Available: <https://linkinghub.elsevier.com/retrieve/pii/B9780443190377000272>
- [5] A. Steane, "Quantum computing," *Reports on Progress in Physics*, vol. 61, no. 2, p. 117, Feb. 1998. [Online]. Available: <https://dx.doi.org/10.1088/0034-4885/61/2/002>
- [6] J. Biamonte, P. Wittek, N. Pancotti, P. Rebentrost, N. Wiebe, and S. Lloyd, "Quantum machine learning," *Nature*, vol. 549, no. 7671, pp. 195–202, Sep. 2017, publisher: Nature Publishing Group. [Online]. Available: <https://www.nature.com/articles/nature23474>
- [7] H. B. McMahan, E. Moore, D. Ramage, S. Hampson, and B. A. y. Arcas, "Communication-Efficient Learning of Deep Networks from Decentralized Data," Jan. 2023, arXiv:1602.05629 [cs]. [Online]. Available: <http://arxiv.org/abs/1602.05629>
- [8] P. Kairouz, H. B. McMahan, and et al., "Advances and Open Problems in Federated Learning," Mar. 2021, arXiv:1912.04977 [cs, stat]. [Online]. Available: <http://arxiv.org/abs/1912.04977>
- [9] D. Gurung, S. R. Pokhrel, and G. Li, "Performance analysis and evaluation of postquantum secure blockchained federated learning," *Computer Networks*, vol. 255, p. 110849, Dec. 2024. [Online]. Available: <https://www.sciencedirect.com/science/article/pii/S1389128624006819>
- [10] D. Gurung and S. R. Pokhrel, "A Personalized Quantum Federated Learning," in *Proceedings of the 8th Asia-Pacific Workshop on Networking*, ser. APNet Kairouz'24. New York, NY, USA: Association for Computing Machinery, Aug. 2024, pp. 175–176. [Online]. Available: <https://dl.acm.org/doi/10.1145/3663408.3665806>
- [11] C. P. Williams, *Explorations in Quantum Computing*, ser. Texts in Computer Science. London: Springer, 2011.
- [12] H. Caesar, V. Bankiti, A. H. Lang, S. Vora, V. E. Liong, Q. Xu, A. Krishnan, Y. Pan, G. Baldan, and O. Beijbom, "nuScenes: A Multimodal Dataset for Autonomous Driving," in *Proceedings of the IEEE/CVF Conference on Computer Vision and Pattern Recognition*, 2020, pp. 11 621–11 631.
- [13] C. Li, N. Kumar, Z. Song, S. Chakrabarti, and M. Pistoia, "Privacy-preserving quantum federated learning via gradient hiding," *Quantum Science and Technology*, vol. 9, no. 3, p. 035028, May 2024, publisher: IOP Publishing. [Online]. Available: <https://dx.doi.org/10.1088/2058-9565/ad40cc>
- [14] S. Behera, M. Adhikari, V. G. Menon, and M. A. Khan, "Large Model-Assisted Federated Learning for Object Detection of Autonomous Vehicles in Edge," *IEEE Transactions on Vehicular Technology*, vol. 74, no. 2, pp. 1839–1848, Feb. 2025.
- [15] M. M. Eid Kishawy, M. T. Abd El-Hafez, R. Yousri, and M. S. Darweesh, "Federated learning system on autonomous vehicles for lane segmentation," *Scientific Reports*, vol. 14, no. 1, p. 25029, Oct. 2024.
- [16] V. Mundheda, Z. Wu, and J. Schneider, "Teacher-guided Off-road Autonomous Driving," *Workshop on Machine Learning for Autonomous Driving*, 2025.
- [17] L. Zhang, Y. Xiong, Z. Yang, S. Casas, R. Hu, and R. Urtasun, "Copilot4D: Learning Unsupervised World Models for Autonomous Driving via Discrete Diffusion," in *The Twelfth International Conference on Learning Representations*, Oct. 2023.
- [18] D. Gurung, S. R. Pokhrel, and G. Li, "Quantum Federated Learning: Analysis, Design and Implementation Challenges," Jun. 2023. [Online]. Available: 10.48550/arXiv.2306.15708
- [19] N. Holohan, S. Braghin, P. M. Aonghusa, and K. Levacher, "Diffprivlib: The IBM Differential Privacy Library," Jul. 2019.

- [20] T. Ji and P. Li, “Less is More: Revisiting the Gaussian Mechanism for Differential Privacy,” *USENIX*, 2024.
- [21] S.-K. Liao, W.-Q. Cai, and et al., “Satellite-to-ground quantum key distribution,” *Nature*, vol. 549, no. 7670, pp. 43–47, Sep. 2017.
- [22] F. Liang, Q. Yang, R. Liu, J. Wang, K. Sato, and J. Guo, “Semi-Synchronous Federated Learning Protocol With Dynamic Aggregation in Internet of Vehicles,” *IEEE Transactions on Vehicular Technology*, vol. 71, no. 5, pp. 4677–4691, May 2022.
- [23] J.-H. Chen, M.-R. Chen, G.-Q. Zeng, and J.-S. Weng, “BDFL: A Byzantine-Fault-Tolerance Decentralized Federated Learning Method for Autonomous Vehicle,” *IEEE Transactions on Vehicular Technology*, vol. 70, no. 9, pp. 8639–8652, Sep. 2021.
- [24] A. Nguyen, T. Do, M. Tran, B. X. Nguyen, C. Duong, T. Phan, E. Tjiputra, and Q. D. Tran, “Deep Federated Learning for Autonomous Driving,” Apr. 2022.
- [25] I. K. Sethi, “Autonomous vehicles and systems - a technological and societal perspective,” *River Publishers*, 2023.
- [26] Q. Xu, L. Zhao, Z. Su, D. Fang, and R. Li, “Secure Federated Learning in Quantum Autonomous Vehicular Networks,” *IEEE Network*, vol. 37, no. 6, pp. 240–247, Nov. 2023.
- [27] N. Kehtarnavaz, N. Groszold, K. Miller, and P. Lascoe, “A transportable neural-network approach to autonomous vehicle following,” *IEEE Transactions on Vehicular Technology*, vol. 47, no. 2, pp. 694–702, May 1998.
- [28] P. Hang, C. Lv, C. Huang, J. Cai, Z. Hu, and Y. Xing, “An Integrated Framework of Decision Making and Motion Planning for Autonomous Vehicles Considering Social Behaviors,” *IEEE Transactions on Vehicular Technology*, vol. 69, no. 12, pp. 14 458–14 469, Dec. 2020.
- [29] C. H. Bennett and G. Brassard, “Quantum cryptography: Public key distribution and coin tossing,” *Theoretical Computer Science*, vol. 560, pp. 7–11, Dec. 2014.
- [30] B. Korzh, C. C. W. Lim, R. Houlmann, N. Gisin, M. J. Li, D. Nolan, B. Sanguinetti, R. Thew, and H. Zbinden, “Provably secure and practical quantum key distribution over 307 km of optical fibre,” *Nature Photonics*, vol. 9, no. 3, pp. 163–168, Mar. 2015.
- [31] E. Biham, M. Boyer, P. O. Boykin, T. Mor, and V. Roychowdhury, “A proof of the security of quantum key distribution (extended abstract),” in *Proceedings of the Thirty-Second Annual ACM Symposium on Theory of Computing*. Portland Oregon USA: ACM, May 2000, pp. 715–724.
- [32] T. Metger and R. Renner, “Security of quantum key distribution from generalised entropy accumulation,” *Nature Communications*, vol. 14, no. 1, p. 5272, Aug. 2023.
- [33] A. Geiger, P. Lenz, C. Stiller, and R. Urtasun, “Vision meets robotics: The KITTI dataset,” *The International Journal of Robotics Research*, vol. 32, no. 11, pp. 1231–1237, Sep. 2013.
- [34] P. Sun, H. Kretzschmar, X. Dotiwalla, A. Chouard, V. Patnaik, P. Tsui, J. Guo, Y. Zhou, Y. Chai, B. Caine, V. Vasudevan, W. Han, J. Ngiam, H. Zhao, A. Timofeev, S. Ettinger, M. Krivokon, A. Gao, A. Joshi, Y. Zhang, J. Shlens, Z. Chen, and D. Anguelov, “Scalability in perception for autonomous driving: Waymo open dataset,” in *Proceedings of the IEEE/CVF Conference on Computer Vision and Pattern Recognition (CVPR)*, June 2020.